Nano Communication Networks 9 (2016) 43–57

Contents lists available at ScienceDirect

Nano Communication Networks

journal homepage: www.elsevier.com/locate/nanocomnet

Characterizing terahertz channels for monitoring human lungs with wireless nanosensor networks

Eisa Zarepour [a,c,*], Mahbub Hassan [a], Chun Tung Chou [a], Majid Ebrahimi Warkiani [b]

[a] School of Computer Science and Engineering, University of New South Wales, Sydney, Australia

[b] Laboratory of Microfluidics & Biomedical Microdevices, School of Mechanical and Manufacturing Engineering, University of New South Wales, Sydney, Australia

[c] AICT Innovation Center, Sharif University of Technology, Tehran, Iran

ARTICLE INFO

Article history:
Received 20 November 2015
Received in revised form
7 September 2016
Accepted 8 September 2016
Available online 19 September 2016

Keywords:
WNSNs
In-vivo communication
Lung monitoring system
Periodic channel
Channel estimation
Nanoscale communication

ABSTRACT

We characterize terahertz wireless channels for extracting data from nanoscale sensors deployed within human lungs. We discover that the inhalation and exhalation of oxygen and carbon dioxide causes periodic variation of the absorption coefficient of the terahertz channel. Channel absorption drops to its minimum near the end of inhalation, providing a window of opportunity to extract data with minimum transmission power. We propose an algorithm for nanosensors to estimate the periodic channel by observing signal-to-noise ratio of the beacons transmitted from the data sink. Using real respiration data from multiple subjects, we demonstrate that the proposed algorithm can estimate the minimum absorption interval of the periodic channel with 98.5% accuracy. Our analysis shows that by confining all data collections during the estimated low-absorption window of the periodic channel, nanosensors can reduce power consumption by six orders of magnitude. Finally, we demonstrate that for wireless communications within human lungs, 0.1–0.12 THz is the least absorbing spectrum within the terahertz band.

1. Introduction

Recent advancements in nanotechnology have made it possible to fabricate sensor nodes below 100 nanometers in size using various types of novel materials. These nanosensors have extraordinary sensing capabilities and can sense a range of information at molecular level. For example, it is now possible to fabricate supersensitive nanoscale sensors that can measure chemical compounds in concentrations as low as one part per billion (ppb) [1]. Medical researchers are already considering the use of nanoparticles for targeted delivery of drugs to infected cells within human body [2,3]. When sensing is combined with these nanoparticles, they can also collect a range of valuable cell-level data for early detection of diseases. Wireless communication for such nanosensors will be a key enabler for such cell-level data collection from human body.

Although wireless communication at nanoscale has not been successfully demonstrated yet, recent simulation studies confirm that these nanosensors may be able to communicate in the terahertz band (0.1–10 THz) using graphene as a transmission antenna [4]. Following this development, in this paper, we present the design of a terahertz Wireless NanoSensor Network (WNSN) for monitoring human lung. The WNSN continuously measures important cell-level data inside lung cells and send them back to the Internet using terahertz communication.

The practicality of the proposed WNSN will critically depend on the transmission power requirements of the nanosensors to reliably forward (upload) data to the sink. If required power for single-hop data upload exceeds what could be practically supplied either through onboard batteries or energy harvesting, more complicated networking architectures, such as multi-hop routing must be considered. As multi-hop communication has significant computing and communication overheads of its own, we focus on duty cycling solutions that would make single-hop communication viable. In particular, we aim to analyze terahertz channel within human

* Corresponding author at: School of Computer Science and Engineering, University of New South Wales, Sydney, Australia.
E-mail addresses: ezarepour@cse.unsw.edu.au, zarepour@ictic.sharif.ir (E. Zarepour), mahbub@cse.unsw.edu.au (M. Hassan), ctchou@cse.unsw.edu.au (C.T. Chou), m.warkiani@unsw.edu.au (M. Ebrahimi Warkiani).

http://dx.doi.org/10.1016/j.nancom.2016.09.001
1878-7789/

lungs and identify unique opportunities that could be exploited to drastically reduce transmission power requirements for nanosensors.

The contributions and novelty of the paper can be summarized as follows:

- We discover that respiration, i.e., the periodic inhalation and exhalation of oxygen and carbon dioxide, causes periodic variation of the absorption coefficient of the terahertz channel. Consequently, transmission power required for reliable communication varies significantly during a respiration cycle. If nanosensors are allowed to communicate at any time during the respiration cycle, transmission power in the order of microwatts would be required to guarantee reliable communication at distance equal to 1 cm, which would be difficult to secure at nanoscale.
- We found a *temporal sweet spot* (will be referred to as *sweet spot* from now on) in respiration cycle when terahertz absorption drops to its lowest values. It is located near the end of inhalation. We show that by exploiting the sweet spots, i.e., completing all communications only during the sweet spot in each cycle, transmission power requirement for nanosensors can be drastically reduced by at least six orders of magnitude.
- We propose an online algorithm for nanosensors to estimate the periodic channel by observing signal-to-noise ratio of periodic beacons broadcast by the nanosinks. Using real respiration data from multiple subjects we demonstrate that the proposed algorithm can estimate the period and sweet spots of the channel with 98.5% accuracy, which allows at least six orders of magnitude power reduction.
- We conduct a frequency-dependent absorption analysis for the entire terahertz band. Our analysis reveals that the effect of respiration cycle is not uniform over all frequencies. In particular, a 20 GHz wide sub-band between 0.1 and 0.12 THz is found to be the least affected. Restricting communication to this sub-band enables further power reduction allowing nanosensors to communicate with only 3 pico watts at a distance of 5 cm.

The rest of the paper is structured as follows. We discuss related work in Section 2. The proposed WNSN for lung monitoring is presented in Section 3. The effect of respiration on the terahertz channel inside human lung is analyzed in Section 4. The proposed channel estimation algorithm that enables exploitation of the sweet spot is presented in Section 5, followed by its evaluation in Section 6. We conclude the paper in Section 7.

2. Related works

Current network protocols and techniques may not be directly applied to WNSNs. In specific, due to the size and energy constraints of nanosensors and also high molecular absorption noise and attenuation in the WNSN channel, designing simple, reliable and energy efficient communication protocols is one of the active research areas in WNSNs [5–13]. We would like to highlight one category of research in this area which is related to current study. It is known that the quality of communication in the terahertz band is frequency sensitive due to sensitivity of the molecular absorption to the frequency [7,10]. That means first, for a given composition different frequency regions absorb the energy differently and second, this absorption pattern over the frequency is composition sensitive, i.e., different compositions have different absorption spectra. As a result, selecting an appropriate frequency range for a given channel composition, i.e., the sub-band with the lowest average absorption have been well-studied in the literature [5–7,10]. However, none of the aforementioned works have studied human lung as the communication medium.

Time-varying WNSNs were first introduced in [10–12] where WNSNs were used for chemical reactor monitoring with the composition of the wireless medium affected by the ongoing reactions constantly taking place in the reactor. Consequently, adaptive communication protocols such as frequency hopping [10] and power adaptation [12,14] have been proposed to provide reliable communication, which is key to improve performance of any WNSNs-based application [11,12]. Our current work with human lungs also deals with time-varying terahertz channel, but the cause of variation is due to human respiration. In addition, the communication channel in the lung is periodic which is not the case in chemical reactors.

Work on the in-vivo WNSNs is rare. In a recent work, a conceptual WNSN for intrabody disease detection has been analyzed in which nanosensors are assumed to be deployed in a hexagonal cell-based architecture in a 3D cylindrical shape [15]. Authors investigate the data transmission efficiency for different transmission methods such as direct and multi-hop. In another recent work, the communication in human skin tissues has been investigated where experimental data for the molecular absorption coefficient of the human tissues has been employed to characterize the quality of communication using the same propagation model that we have used [16]. In both of these works, the composition of the communication channel between nanomotes are assumed fixed while in the current study, we try to characterize the time-property of the terahertz within human lung and design efficient protocols that utilize the respiratory data to smartly select the sweet spots.

Challenges and opportunities of using WNSNs for human lung monitoring were first discussed in our preliminary work [17]. However, as compared with [17], this paper has significant extensions and new materials summarized as follows. First, in [17] only local communication within an alveolus cell of a lung has been investigated while in the current study the terahertz channel through the entire lung has been analyzed. More analyses and graphs are also presented on the channel conditions including, attenuation, molecular noise, SNR and BER. Second, in [17] the respiration cycles were assumed deterministic and known. In current study, we have relaxed this assumption, which is more realistic as evidenced by real datasets. We have proposed an algorithm to estimate respiration period and analyzed its accuracy using real datasets. Finally, [17] only investigates the power reduction opportunities by exploiting the sweet spots while in the current study we explore further power saving opportunities by identifying specific frequency sub-bands within the terahertz band that have lower absorption coefficients than other sub-bands.

3. Proposed WNSN for lung monitoring

WNSNs are expected to sense and control important physical processes right at the molecule level delivering unprecedented performance improvement of medical, industrial, biological, and chemical applications [18,19]. Indeed, researchers now believe that WNSNs can potentially be deployed inside human body for more detailed real-time health monitoring, targeted drug delivery, and so on [18,2].

It is well-known that by monitoring the composition of the human lung, many diseases such as asthma, bronchiectases and even lung cancer can be detected at the very early stage of development [20]. For example, volatile organic compounds (VOCs) in breath are recently found as a novel biomarker that can provide precise information for quick diagnosis of many lung diseases such as asthma [21] and lung cancer [22–24].

In addition, there is a significant progress in developing nanoscale biosensors that are able to efficiently measure the lung

diseases biomarkers [25–28]. For example, a silicon nanowire-based field effect transistor has been reported that is able to detect VOCs in low concentration as few as ppb [26]. Another study has demonstrated that a nanosensor consisting of an array of 14 gold nanoparticle electrodes is able to detect many types of VOCs [27].

Taking these remarkable advancements into consideration, in this work, we propose a WNSN to remotely monitor human lung at the molecular level. We first describe the lung structure followed by the proposed WNSN-based architecture for remote lung cell monitoring.

3.1. Lung structure

The human lung is the organ of respiration, composed of a pair of large spongy organs optimized for gas exchange between the blood and the air (Fig. 1(a)). Each lung consists of millions of alveolus cells, the functional units of the lungs that permit gas exchange. Alveolus are found in small clusters called alveolar sacs at the end of the terminal bronchiole (Fig. 1(b)). A thin layer of connective tissue underlies and supports the alveolar cells. At the membrane of alveolus cells, gas exchange occurs between the air and blood through the extremely thin walls of the alveolus and capillary (Fig. 1(c)).

Upon inspiration, the intra-alveolar pressure change around 5–6 mmHg within one respiration cycle due to relaxation of the intercostal muscles and diaphragm. Due to the same reason, the radii of an alveolus periodically varies between about 0.1 and 0.2 mm. We will later use these variations to harvest energy for our nanomotes.

Our proposed WNSN-based lung monitoring architecture is presented next.

3.2. Proposed WNSN architecture

The proposed system aims to measure and report biomarkers that can help detect lung-related diseases. We target sparse sampling from several alveoli colonies that have been selected across both left and right lungs. For this purpose, we propose a hierarchical WNSN-based solution which includes four levels as depicted in Fig. 1.

At the lowest level, we assume that we can deploy a nanomote within each targeted alveolus cell to collect data from the cell. We refer to these nanomotes as '*nanocollectors*'. Nanocollectors can be attached to the cell walls by using some bioengineering techniques such as artificial bacteria [29]. Each nanocollector has been equipped with a nanoscale energy harvester [30] to harvest energy from pressure variation and cell wall movement during the respiration cycle; a nanosensor [31] to measure the target biomarkers in the exchanged gases; a nanomemory [32] to save the detected marker; a nanoprocessor [33] to run the required algorithm and a nanotransmitter [4] to transfer the recorded markers wirelessly to a nanoscale remote station or *nanosink*. A schematic of the proposed nanocollector has been depicted in Fig. 1(d).

In the next level, two nanosinks would be deployed at the central points of both left and right lungs to receive signals from many nanocollectors. The nanosinks are similar to nanocollectors in construction, except they do not have any sensor but instead have an extra energy harvester that can scavenge energy from RF waves. RF energy harvesters would allow charging the nanosinks from outside the human body. Nanosinks transmit the data received from the nanocollectors to the next level, which is a *macrosink* patched to the chest. The macrosink relays the data received from nanosinks to the user device, a smartphone for example. The data would be processed by a special software on the device and the results would be displayed on the user's device monitor. For further analysis or to keep the person's record on a cloud, the data could be transferred to a remote health server via Internet.

From the foregoing description of the proposed WNSN, we see that the nanosinks and the macrosink can be powered easily using wireless (RF) charging as they are located closer to outside of the body. However, the tiny nanomotes buried deep inside the alveolus cells cannot be charged wirelessly from outside. The only viable option for the nanomotes is to power themselves using the pressure energy harvester they are fitted with and use the scant harvested energy wisely to deliver data reliably to the nanosinks. This poses a formidable communication challenge due to the significant channel absorption in THz. Indeed, the current work aims to address this communication challenge by exploring low absorption time and frequency windows inside human lungs. Before presenting our solution though, in the following section, we first take a look at the energy harvesting opportunities and power requirements for the nanomotes.

3.3. Powering of nanomotes

In this section, the power requirement of the proposed nanomotes and also possible opportunities to harvest energy from ambient environment (in-vivo) will be discussed.

3.3.1. Power requirement

The major power hungry components in our proposed architecture are the sensor and transmitter. The required power to reliably transfer data from the nanocollectors to the macrosink depends on few parameters such as the distance between the devices and the composition of the wireless medium, which will be discussed in Section 4.

The exact power requirement of the nanosensor depends on the targeted diseases that the proposed architecture aims to discover. Typically, the power requirement for nanoscale chemical/biological sensors varies from less than few nW to few μW [35]. However, there is a research trend in the literature trying to design self-powered nanosensors using some physical/chemical phenomena that create charge in the sensor when it exposes to different materials [36–40]. For example, *triboelectric effect* has been employed to design self-powered nanosensors [36]. The triboelectric effect is a phenomenon that contact between two materials with different triboelectric polarities creates surface-charge transfer. Different materials create different charges that can be used as a signature to detect the contacted material. As another example, a biological sensor that is able to detect dopamine[1] has been manufactured and tested [36]. Self-powered cholesterol [38], glucose [39,40] and VOCs [41] biosensors have been also successfully demonstrated.

3.3.2. Energy harvesting

In vivo biomechanical sources such as cell movement and pressure variation are the most promising sources to harvest energy for biomedical and health-care applications [42,30,43]. Biochemical reactions inside human body such as cell respiration can be also considered as a potential source whereas nanogenerator convert the chemical energy of glucose and oxygen in biofluid into electricity [44].

In our proposed lung monitoring system, the nanocollectors can use a piezoelectric nanogenerator to either harvest energy from the motion due to alveolus cell movement or pressure variation during the respiration process. According to the literature, up to

[1] A class of aromatic amines that plays an important role in the central nervous renal, and hormonal systems.

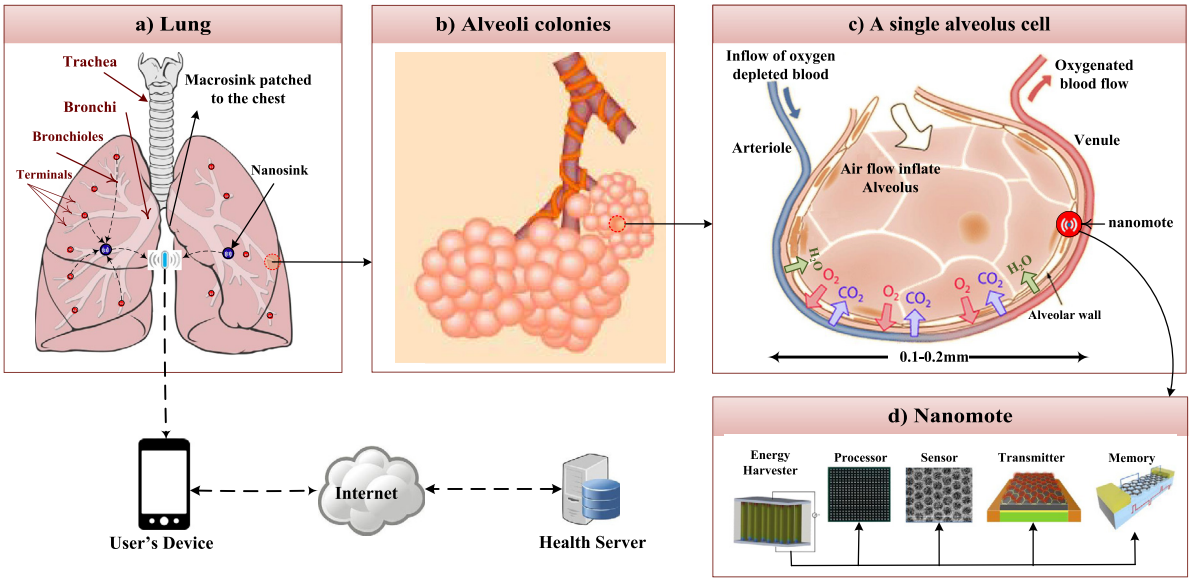

Fig. 1. A schematic architecture of the proposed lung monitoring system via WNSN.
Source: adapted from [4,30–34].

few pW (10^{-12}) can be harvested from motions of human organs in each respiration cycle using a flexible piezoelectric nanogenerator of one square micron size [30].

The nanosinks need more power as they need to collect data from many nanocollectors and transmit data to the macrosink. RF energy harvesting might be an option for nanosinks, i.e., macrosink feed the nanosinks via wireless RF transmissions.

3.4. Respiratory system

The quality of communication in WNSN is strongly affected by the composition of the communication medium [46] which will be explained in more details in Section 4. It is then important to identify the composition of the medium in the proposed architecture. Because the respiratory system affects the composition of the lung (our communication medium), in this section we briefly overview the respiratory system.

The blood circulatory system circulates the blood through the body; carrying oxygen to the cells; collecting the excess water and CO_2 which has been produced during cell respiration; and carries them to the alveolus cells in the lungs (Fig. 1(c)). This process affects the composition of the all alive cells including the alveolus cells in lung. Table 1 shows the composition of the in/exhaled air. While less than 0.04% of the inhaled air is CO_2, the exhaled air is composed of 4%–6% CO_2. It also shows that the water molecules varies from less than 1% to 3%–5% during one respiration cycle. The normal respiratory rate, known also as *eupnea*, varies with age, activities, illness, emotions and drugs [47, pp. 291] and is measured as the number of breaths taken per minute (bpm). For example, at rest and healthy condition it could vary from 12 bpm for an adult to 55 bpm for an infant. In medicine, *capnography* is the method to measure the amount of CO_2 in the inhaled and exhaled air. The signal that is called *capnogram* represents the concentration or partial pressure of CO_2. Fig. 2 shows a snapshot of the capnogram of a given subject that contains two respiration cycles, extracted from CapnoBase[2] [48,49]. It shows that the CO_2 concentration fluctuated within one respiration cycle. It starts at a low level at the beginning of exhalation and raises to its maximum before inhalation starts.

Table 1
The composition percentage of exhaled and inhaled air [45].

	N_2	O_2	CO_2	H_2O	Others
Inhaled air	78	21	0.05	<1	<0.1
Exhaled air	78	13–16	4–6	3–5	<0.1

Fig. 3 shows 60 s snapshot of real capnograms of six different subjects with age ranges from 1 to 59 years that have been obtained while the cases were all spontaneously breathing, extracted from CapnoBase. The min/max CO_2 and pulse width (duration) is different for different subjects. The respiration also change the lung volume. The amount of air that usually exists in the lungs at the end of a regular exhalation is called *functional residual volume* (FRV). The amount of air that would be exchanged during a regular inhalation/exhalation is called *tidal volume* (TV). Lung related volumes such as FRV and TV depend on many parameters such as age, gender, weight, height and exercise. [50]. For example, based on the age and weight of the subject 4, his FRV and TV would be approximately 1.1 and 0.3 l, respectively.

3.5. WNSN communication medium

In the proposed human lung monitoring system, there are two types of wireless media including wireless communication between nanocollectors and the nanosinks through the alveoli (*alveoli medium*); and between the nanosinks and the macrosink (*ToMacro*). In this paper, we investigate the alveoli medium which is the most challenging medium as its composition periodically varies due to respiration process.

The communication between nanocollectors and the nanosinks is mainly affected by the alveoli composition that consists of three main layers including the existing gases in the alveolus cell membranes, i.e. exchanged gases; tissues (airways and connective tissue which separates alveolus cells); and blood. On average, around 90% of the lung volume consists of the gaseous molecules [51, p. 1124] but the relative thickness of these three layers and their compositions vary over time due to respiration system which will be studied in more details in Section 4.2.

[2] CapnoBase which was developed at the University of British Columbia is an online database of respiratory signals obtained from capnography and spirometry. It provides respiratory signals such as inhaled and exhaled carbon-dioxide (capnogram), respiratory flow and pressure. CapnoBase contains many 8 min real capnogram traces for different subjects in different ages.

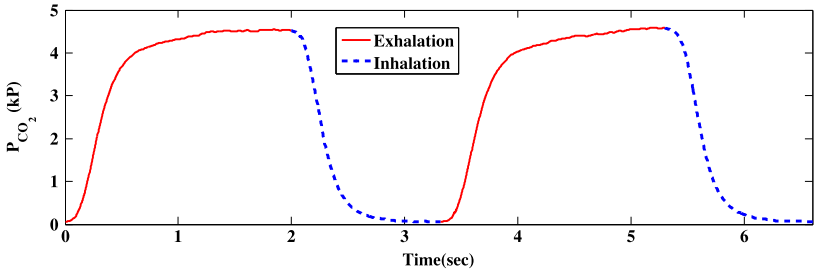

Fig. 2. The capnogram for two respiration cycles showing the inhalation and exhalation phases.

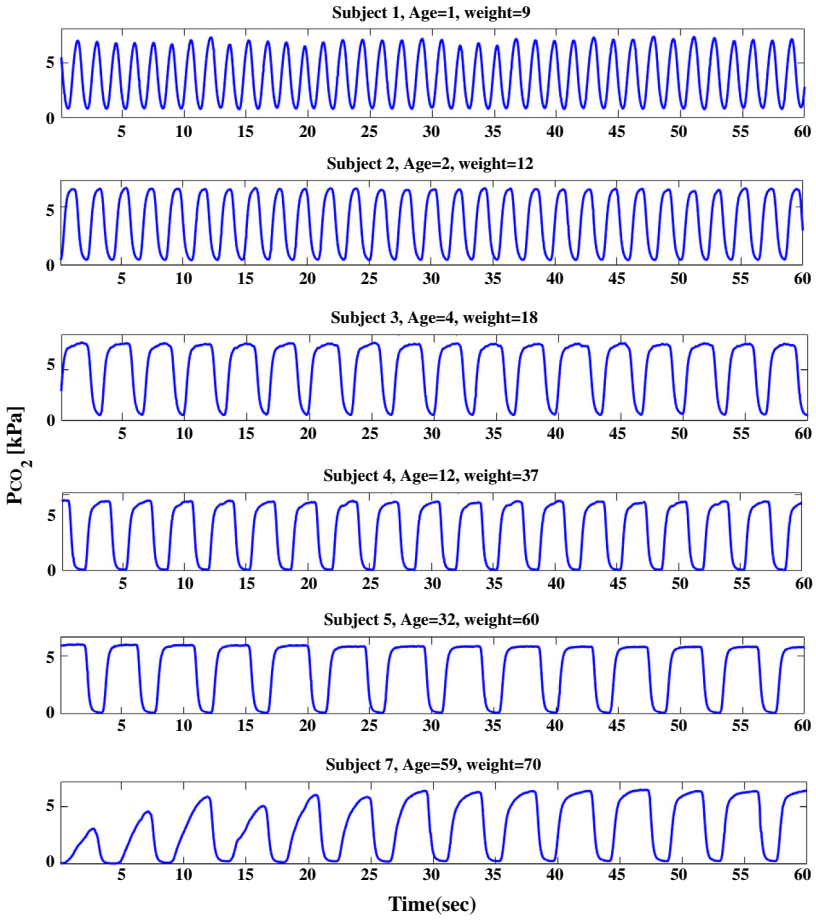

Fig. 3. Variation of the CO_2 during the respiration in six subjects within one minutes that have been experimentally measured [49].

4. THz channel characterization for human lungs

In this section, we aim to characterize the THz communication within the human lung or for the *alveoli medium* to be precise. We first present a time-varying multi-layer THz channel model, followed by its evaluation using real capnogram data. A key outcome of this study is the revelation of a periodic THz communication channel where the absorption increases and decreases periodically due to respiration.

4.1. Time-varying multi-layer THz channel model

Radio communication in terahertz band is affected by the chemical compositions of the medium in two different ways. First, radio signal is attenuated because molecules in the channel absorb energy in certain frequency bands. Second, this absorbed energy is re-radiated by the molecules which creates noise in the channel [46]. For a given chemical molecule of S_i, this phenomenon is frequency sensitive and characterized by its molecular absorption coefficient $K_i(f)$ at frequency f. For a radio channel consisting of N chemical species $S_1, S_2, \ldots, S_N$. The overall absorption coefficient of the medium at frequency f is given as:

$$K(f) = \sum_{i=1}^{N} m_i \times K_i(f) \tag{1}$$

where $K_i(f)$ is the absorption coefficient of molecule i at the frequency f and m_i is the mole fraction, i.e., ratio of the molecule i.

First, let us look at the absorption coefficient of each individual constituent molecules of the lung as our communication medium. The lung consists of three main layers including the exchanged gases (mainly O_2, N_2, CO_2 and water vapor), connective tissues and blood vessels. We use HITRAN database [52] to extract absorption coefficient of the gaseous species but the absorption coefficient of other species are not available in HITRAN. However, the optical properties of human blood over 0.1–1.8 THz has been experimentally measured in [53] and the absorption coefficient of the lung

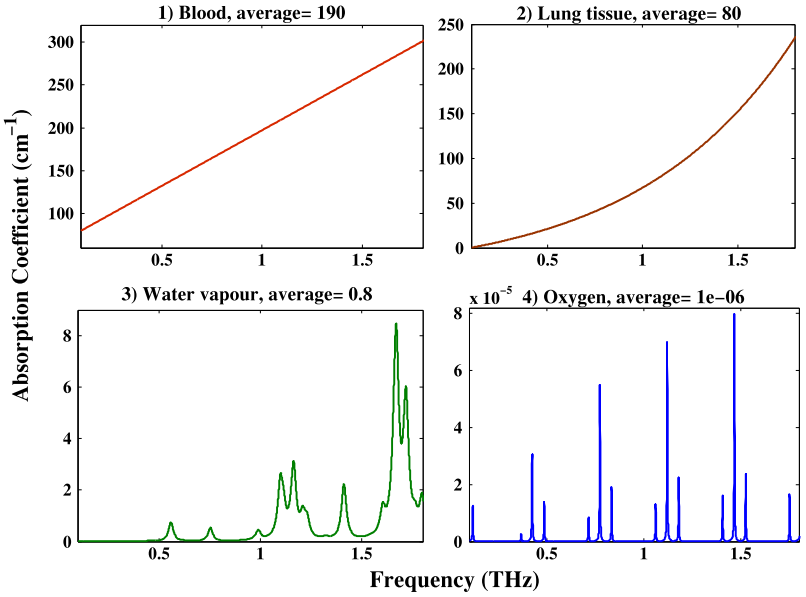

Fig. 4. Absorption coefficients for the main existing molecules in lung over 0.1–1.8 THz. The absorption coefficient of other gaseous molecules (N_2, CO_2, Ne, He and Ar) are almost zero.

tissues has been reported in [54] over 0.1–1.8 THz. As the absorption coefficient of the blood and tissue have been only reported over 0.1–1.8 THz, we limit our study to this sub-band. Fig. 4 shows the absorption coefficient of four main molecules that affect the quality of communication within human lung over 0.1–1.8 THz. It shows that the main absorbent molecules are human blood and tissues with average absorption of 190 cm^{-1} and 80 cm^{-1}, respectively. Based on HITRAN database, N_2 and CO_2 and other gases in the inhaled air such as Ne, He and Ar do not absorb the THz signal over 0.1–1.8 THz and their absorption coefficients are almost zero.

Nevertheless, the thickness of different layers and also the concentration of the gaseous molecules in the lung vary over time due to respiration. We therefore consider a multi-layer radio channel with possible time-varying chemical composition in each layer. We assume there are M layers with $\lambda_j(t)$ denoting the thickness/proportion of layer j at time t. Then, the medium absorption coefficient $K(t, f)$ at time t and frequency f is:

$$K(t,f) = \sum_{j=1}^{M} \frac{\lambda_j(t)}{\Lambda} \sum_{i=1}^{N} m_{j,i}(t) \times K_i(f) \tag{2}$$

where $m_{j,i}(t)$ is the mole fraction of chemical species S_i in layer j at time t and $K_i(f)$ is the absorption coefficient of molecules i at the frequency f. Λ is the total thickness of all the layers, i.e., the distance between transmitter and receiver. The attenuation at time t, frequency f and a distance d from the radio source is [46]:

$$A(t,f,d) = e^{K(t,f)d} \times \left(\frac{4\pi f d}{c}\right)^2. \tag{3}$$

The receivers usually encounter with few types of noises including the thermal noise (N_{Thermal}) generated by the thermal agitation of the charge carriers; electronic noise (Elec) from receiver input circuits and ambient noise from the environment. The ambient noise in terahertz channel is mainly originated by the molecular absorption noise (N_{abs}) which is due to re-radiation of the absorbed energy by the molecules in the channel [55,56]. The total noise power at the receiver therefore is:

$$N = N_{abs} + N_{\text{Thermal}} + N_{\text{Elec}} + N_{\text{Others}} \tag{4}$$

where N_{Others} is the noise from other probable sources. N_{thermal} and N_{Elec} depend on the receiver's technology in use. There are some promising evidences that shows the Graphene-based nanoscale transceivers have a very low thermal noise that means molecular noise is expected to be the dominant source of noise in the channel [56]. The power spectral density (PSD) of molecular absorption noise, $N_{\text{abs}}(t, f, d)$ is given by [46]:

$$N_{\text{abs}}(t,f,d) = k_B T_0 (1 - e^{-K(t,f)\times d}) \tag{5}$$

where T_0 is the reference temperature 296 K and k_B is the Boltzmann constant. Let $U(t, f)$ be the power spectral density of the transmitted radio signal at time t and frequency f. The signal-to-noise ratio (SNR) at time t, frequency f and distance d is:

$$\text{SNR}(t,f,d) = \frac{U(t,f)}{A(t,f,d)N_{\text{abs}}(t,f,d)}. \tag{6}$$

Consider a radio channel consisting of two nodes separated by a distance d, then at time t, the Shannon capacity over a sub-channel from B_1 to B_2 Hz is:

$$\text{Capacity}(t,d) = \int_{B_1}^{B_2} \log_2(1 + \text{SNR}(t,f,d))df. \tag{7}$$

Assuming on–off keying (OOK) [57] as the modulation schema, the average error probability (BER) at time t and distance d can be expressed as [13,58]:

$$\text{BER}(t,d) = \int_{B_1}^{B_2} Q\left(\sqrt{\text{SNR}(t,f,d)}\right) df \tag{8}$$

where $Q(x)$ is defined as:

$$Q(x) = \int_x^{\infty} \frac{1}{\sqrt{2\pi}} e^{\frac{-x^2}{2}} dx.$$

Over a given period of time, i.e. N discrete time stamps, the average BER at distance d can be obtained as:

$$\text{BER}(d) = \frac{\sum_{i=1}^{N} \text{BER}(t_i, d)}{N}. \tag{9}$$

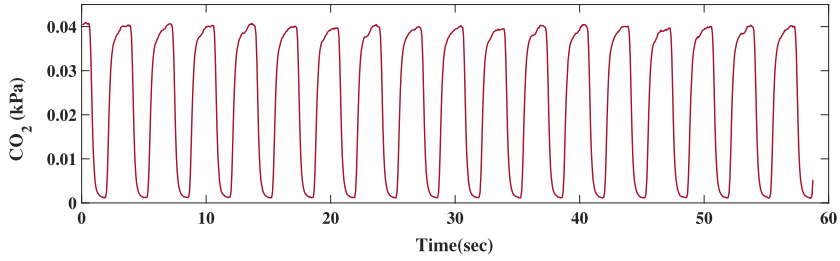

(a) Capnogram, CO_2 partial pressure (kPa).

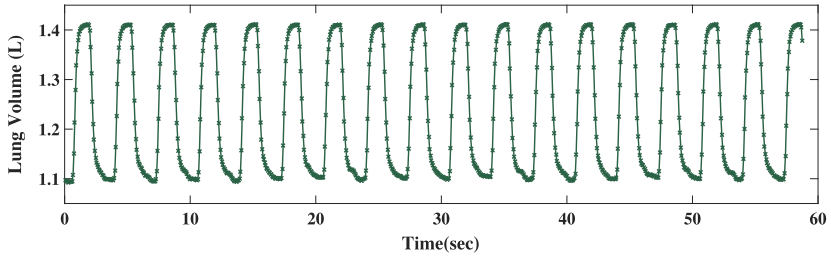

(b) Lung volume variation (Liters).

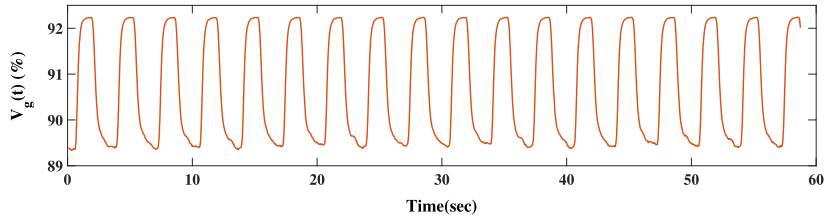

(c) The variation of the proportion of gaseous molecules (%).

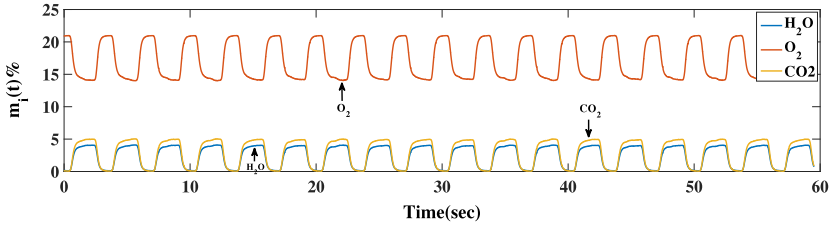

(d) Alveoli gas composition.

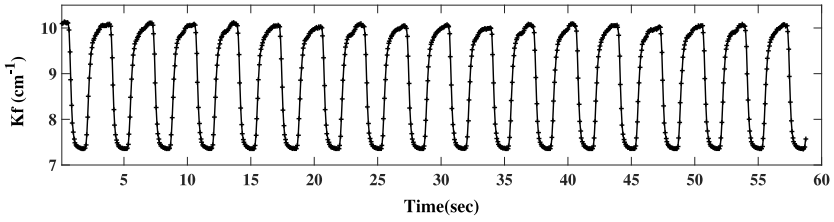

(e) Absorption coefficient (cm^{-1}).

Fig. 5. Lung simulation for subject 4.

4.2. Simulation with real capnogram data

Now, we are ready to analyze the quality of communication between nanocollectors to the nanosinks, i.e., alveoli medium. First, we simulate the variation of lung volume and composition using the capnogram data of the fourth subject (male, 12 years, 37 kg weight). His capnogram over 60 s from CapnoBase [49] has been depicted in Fig. 5(a).

On average, around 90% of the lung volume consists of the gaseous molecules [51, p. 1124] but it varies during the respiration. The lung volume variation, $\Delta V(t)$, can be readily calculated as:

$$\Delta V(t) = C_L \times \Delta P(t) \tag{10}$$

where $\Delta P(t)$ is the intra-alveolar pressure at time t (that can be approximated by the capnogram data), C_L is lung compliance coefficient that is defined as the change in lung volume per unit change in intrapulmonary pressure [59], usually between 0.1 and 0.2. Using the capnogram of subject 4 and Eq. (10), Fig. 5(b) shows that the lung volume changes between 1.1 and 1.4 l periodically. This variation changes the relative thickness of three constituent

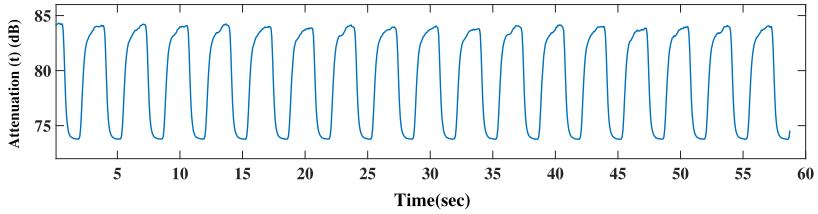

(a) Attenuation.

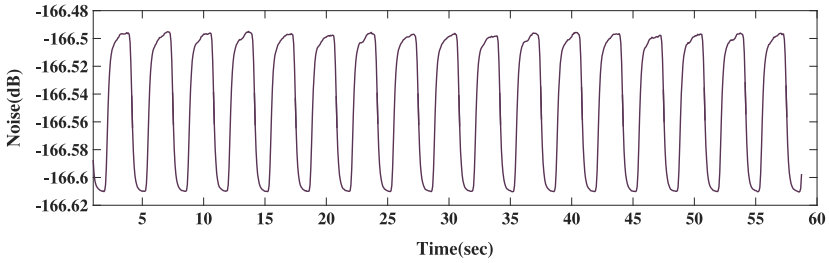

(b) Molecular absorption noise.

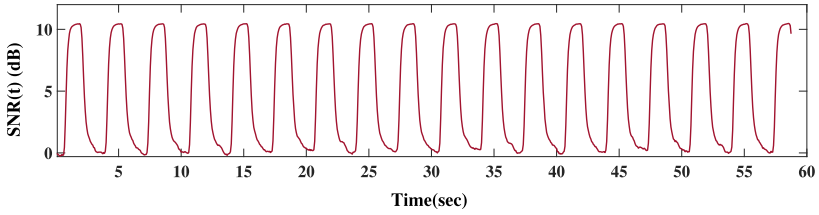

(c) Signal to noise ratio.

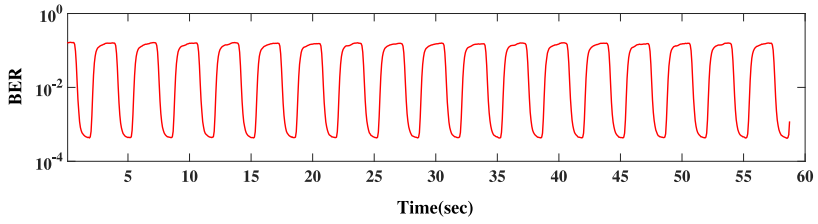

(d) Bit error rate.

Fig. 6. Channel status over 60 s for subject 4, (a) attenuation (b) molecular absorption noise (c) SNR and (d) BER for a transmission power equal to 1 pW and distance 5 mm between two nearby nanocollectors. The quality of communication in the channel periodically changes.

layers of the lung (gas, tissue and blood). The relative thickness of gaseous layer at time t, λ_g, would be:

$$\lambda_g(t) = \frac{V_g(t)}{V_g(t) + V_{b+t}(t)}$$

where $V_{b+t}(t)$ and $V_g(t)$ are respectively, the volume of blood plus tissue[3] and air in the lung at time t. $V_{b,t}(t)$ is equal to $0.1 \times V_g(t)$ and $V_g(t)$ would be:

$$V_g(t) = V_g(t-1) + \Delta V(t).$$

Fig. 5(c) shows that the average proportion of gaseous layer (V_g) varies from 92.25% at the end of regular inhalation to 89.25% at the end of regular exhalation. The maximum and minimum relative thickness of blood/tissue, V_{b+t} is also 10.75% and 7.75%.

While the total volume of gas in the lung is variable, the composition, i.e., the concentration of each gas is also variable over time.[4] In addition, the membrane of alveolus cells is mainly affected by the gas exchange process in the lung. In order to investigate the effect of respiratory system on the composition of the alveolus cells, we need to obtain the variation of the main exchanged gases inducing H_2O, CO_2, O_2 and N_2. We therefore use data from Table 1 and the capnogram data (CO_2 variation) to simulate the gas exchange in the alveolus cell. Fig. 5(d) shows the variation of mole fraction, i.e., concentration of different gaseous molecules during the gas exchange process in the alveolus cells for subject 4 in 60 s. As it can be seen, the concentration of CO_2, O_2 and water vapor is dynamic. The nitrogen is fixed and around 78% which has not been depicted.

Having the relative thickness of the constituent layer of the lung and the composition variation of the gaseous layer over time, we use Eq. (2) to calculate the absorption coefficient of the medium (Fig. 5(e)) which varies approximately from 7.25 to 10.25 cm^{-1} per respiration cycle.

[3] For simplification, we assume the relative thickness of blood and tissues are equal.

[4] The composition of blood and tissue have a small variation over time which are ignored in this study for simplification but will be studied in the future works.

As mentioned in Section 4.1, absorption coefficient characterizes the quality of communication in the channel, so we expect variation in path loss, noise and SNR. We assume a transmitted power equal to 1 pW (10^{-12} W) and a distance equal to 5 mm between nanocollectors and the nanosink.[5] Following Eqs. (3)–(8), Fig. 6 shows the resulting attenuation, molecular noise, SNR and BER in the medium. We would like to highlight two main points. First, Fig. 6 shows that all the channel metrics (except noise) have significant variations which is due to respiratory system. The total path loss in each respiration cycle averagely varies between 73.5 dB and 84.5 dB which finally translate to variation in SNR (between 0 and 10.5) and BER (between 10^{-1} and 3^{-4}). In addition, molecular noise (Fig. 6(b)) has a negligible variation because it is always close to it maximum possible value ($K_B * T0$) due to high absorption in the channel. Second, the channel status is periodic whose period is regulated by the respiratory rate. In addition, the path loss, noise and BER in the channel are minimum when the lung contains the maximum amount of gas at the end of inhalation and the proportion of the tissue/blood is minimum.

As it can be seen in Fig. 6, the quality of communication (SNR) is dynamic over time and periodically switch between good state and bad states. However, in each respiration cycle, near the end of inhalation, there is a temporal sweet spot that absorption drops to its lowest values and SNR has the highest value (Fig. 7). It is clear that power consumption of nanosensors can be significantly reduced by uploading data only during these sweet spots. However, how to identify the beginning and end of sweet spots is challenging for resource constrained sensors. In the following section, we propose and evaluate a sweet spot estimation algorithm that requires minimal resources for implementation.

5. Sweet spot estimation algorithm

The aim of this section is to propose an online algorithm for nanocollectors to estimate the period of the channel in order to exploit the sweet spots. We assume that time is divided into frames of duration T_f and in the beginning of each frame, the nanosinks send beacons for a fixed duration of time T_b with T_f much longer than T_b. During the beaconing duration, nanocollectors measure the SNR of the received beacons. They then use the SNR trace to estimate the period and the timings of the sweet spots, which can be used to estimate the occurrence of sweet spots in the future. An advantage of this method is that continuous beaconing is not required. Consider an alternative scheme where nanocollectors send when the channel is good and keep sending until the channel quality drops below a threshold. After that, the nanocollectors keep listening to the channel until it is good again. Although this approach is simple, it requires nanosinks to continuously broadcast beacons across the lungs which will exhaust the power of the nanosinks and nanocollectors due to continuous channel sensing.

In order to limit the beaconing and channel sensing, we take the periodic property of the channel into account and propose a simple method for nanocollectors to exploit the sweet spots with minimum resources. First, we explain how sweet spot can be obtained for a given respiration cycle. We then propose a method to extend the extracted sweet spot of a respiration cycle to the future cycles. Finally, we analyze the complexity and overhead of this method.

[5] We will study higher distances in Section 6.

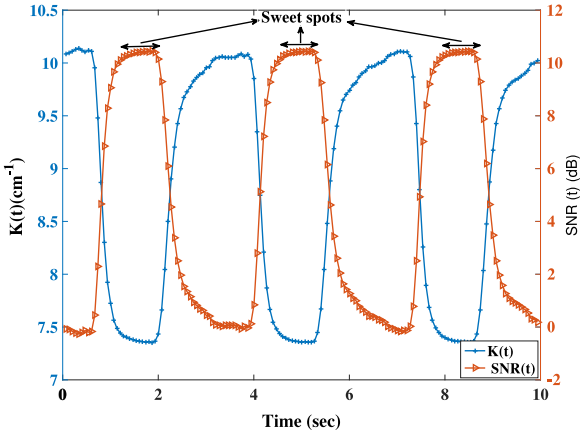

Fig. 7. SNR is a good estimator for the absorption coefficient to exploit sweet spots.

5.1. Sweet spot exploitation for one cycle

Let SNR(t) denote the SNR at time t. Assuming that we know the maximum possible SNR is $\text{SNR}_{\max}$, then we can define the sweet spot as the collection of times over which the $\text{SNR}(t) \geq \eta\ \text{SNR}_{\max}$ where $0 < \eta \leq 1$ is a user defined parameter. If η is big, the width of the sweet spot window will be small and vice versa.

As the channel is periodic, our proposed method aims to use the sweet spots of a given respiration cycle to estimate the sweet spot periods for future cycles which will be introduced in next section.

5.2. Description of the algorithm

The respiration cycle durations for a given person under different health and activity conditions (rest, walk, run, etc.) could be different. However, our investigation using real 8-min lung capnogram profiles of 40 different subjects extracted from CapnoBase database [49] shows that the average period in a given condition (here rest) has a small variance (around 5%). For example, we plot the cycle durations of subject 4 over 8 min (140 cycles) in Fig. 8. As it can be seen, the duration varies between 3.31 and 3.4 s with a standard deviation of 0.015. Based on these observations, it seems that average respiration period over a given duration time of can be used as a good estimation for each individual cycle time if the subject's condition does not change.

The details of the algorithm is given in Algorithm 1. The algorithm takes in three inputs. The first input is the SNR trace measured by the nanocollector over the beaconing interval. The trace consists of L ordered pairs $(t(i), SNR(i))$ $(i = 1, 2, \ldots, L)$ where $SNR(i)$ is the SNR of the beacon received at time $t(i)$. The second input is the parameter η. The third input is the beacon duration T_b which is known to both the nanocollectors and the nanosinks.

The proposed algorithm aims to estimate a few parameters which enable the nanocollector to estimate when future sweet spots happen. Note that a sweet spot begins when the SNR rises above the threshold $\eta\ \text{SNR}_{\max}$ and ends when the SNR drops below the threshold $\eta\ \text{SNR}_{\max}$. We say that a sweet spot is *complete* if both its beginning and end fall within the beaconing duration. The algorithm counts the number of complete sweet spots in the SNR trace and use this count to estimate the average respiration period $\overline{T}_p$. Furthermore, the algorithm returns the time instances $\hat{t}_1$ and $\hat{t}_2$ which are the beginning and end of the last complete sweet spot in the SNR trace. Given these outputs, the nanocollectors will estimate that subsequent sweet spots to be beginning (resp. ending) at time instances $\hat{t}_1 + i\overline{T}_p$ $(\hat{t}_2 + i\overline{T}_p)$ where $i = 1, 2, 3, \ldots$.

Algorithm 1: Respiration period estimation from SNR signal.

Inputs: SNR trace $(t(i), SNR(i))$ $(i = 1, 2, \ldots, L)$. Parameters η and T_b
Calculate $SNR_{max} = max_{i=1,\ldots,L} SNR(i)$
Calculate $\lambda = \eta\ SNR_{max}$
Integer variable *count* = 0 // count is the number of complete cycles
Boolean variable $within = 0$
// $within = 1(0)$ if the last time instance is inside (outside) a sweet spot
for *i from L to 1 step* -1 **do**
  if $within == 0$ **then**
    if *(SNR(i-1)* $> \lambda$ *) and (SNR(i)* $<= \lambda$ *)* **then**
      // t(i) This is the end time of a sweet spot
      within = 1
      if *count* $== 0$ **then**
        $\hat{t}_2 = t(i)$
  else
    if *(SNR(i-1)* $< \lambda$ *) and (SNR(i)* $>= \lambda$ *)* **then**
      // t(i) This is the beginning time of a sweet spot
      within = 0
      if *count* $== 0$ **then**
        $\hat{t}_1 = t(i)$
      count = count + 1
$\overline{T}_p = \frac{T_b}{count}$
Outputs: $\overline{T}_p, \hat{t}_1, \hat{t}_2$

The algorithm first determines the maximum SNR over the trace and use this to calculate the SNR that defines the sweet spot threshold. It then scans the SNR trace backwards in time so that it can locate the beginning and end of the last complete sweet spot in the trace, which are output in the variables $\hat{t}_1$ and $\hat{t}_2$. The variable *count* is used to accumulate the number of complete sweet spots in the SNR trace. The period of a respiration cycle is estimated by dividing the beaconing duration T_b by the number of complete sweet spots. Our proposed algorithm therefore ignores the fractional cycles in the SNR trace. We show with empirical data in Section 6.1 that this approximation does not cause much inaccuracy.

5.3. Overhead and complexity of the proposed algorithm

The energy overhead of the proposed algorithm depends on two parameters namely number of transmitted beacons (L in the algorithm) and the distance d between the nanosinks and nanocollectors. We choose the beaconing interval T_b to be 30 s so that sufficient number of cycles are included. With a beaconing interval of 100 ms, the number of beacons sent by a nanosink is $L = 300$. The distance between nanocollector and the nanosinks depends on the distribution and density of the nanocollectors in each lung. Here, we assume an average distance of 5 cm between a nanocollector and a nanosink. We will show in Section 6.3 that if nanosinks use the 100–102 GHz frequency range to broadcast the beacons then they need only around 70 pico Watts per beacon to successfully deliver the beacons at distance of 5 cm. This amount of power is reasonable for nanosinks.

Regarding the complexity of the proposed algorithm, nanocollectors need to save and process an SNR trace with $L = 300$ data points. The storage requirement is linear in L. The proposed algorithm needs to scan the trace twice, once for computing the maximum and once for the for-loop in Algorithm 1. The algorithmic complexity is linear in L. The currently available nanoscale memories can read/write a single bit in less than few nanoseconds [60,61] and this satisfies our application's requirement. Regarding the processing time, theoretically, the switching frequency of nanoscale transistors such as carbon nanoribbon and carbon nanotube transistors are around 10 THz [62]; this is good enough for our application.

6. Evaluation

In this section, we use simulation experiments to evaluate the efficacy of the proposed terahertz channel estimation and sweet spot exploitation algorithm in reducing the transmission power requirement of the WNSN. The goals of the evaluation are three fold: (1) investigate the accuracy of the proposed channel estimation algorithm for tracking the periodic channel and the sweet spots using real respiration data, (2) quantify the power reduction opportunities by exploiting the sweet spots, and (3) explore further power saving opportunities by identifying specific frequency subbands within the terahertz band that have lower absorption coefficients than other subbands.

6.1. Accuracy of sweet spot detection

Recall that sweet spot exploitation relies on how accurately the sensors can estimate the periods of upcoming respiration cycles. We use the metric *mean absolute percentage error* (MAPE) to measure the error in estimating the respiration period (cycle time), which affect the sweet spot detection in future cycles. We use the first 30 s of an eight minute respiration trace of a given person (from capnoBase [49]) to compute the estimated average period, $\overline{T}_p$ using Algorithm 1. Then, we extract the true periods of all remaining cycles in the trace (the 7.5 min) using the *pulseperiod* function of MATLAB signal processing toolbox. Period estimation error is obtained as:

$$MAPE = \frac{1}{N} \sum_{i=1}^{N} \left| \frac{\overline{T}_p - T_{p,i}}{T_{p,i}} \right| \tag{11}$$

where N is the number of cycles in the remaining 7.5 min trace and $T_{p,i}$ is the true period of cycle i. Period estimation accuracy is obtained as $1 - MAPE$. Multiplying the number by 100 gives the accuracy in percentage.

To evaluate MAPE of the proposed estimation algorithm, we choose 15 subjects among available subjects in CapnoBase and

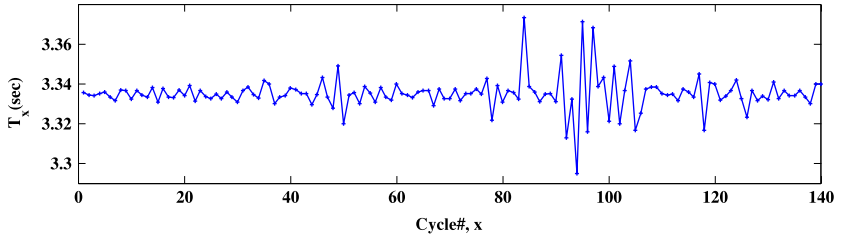

Fig. 8. The cycle durations over 140 cycles (8 min). The standard deviation of this dataset is 0.015.

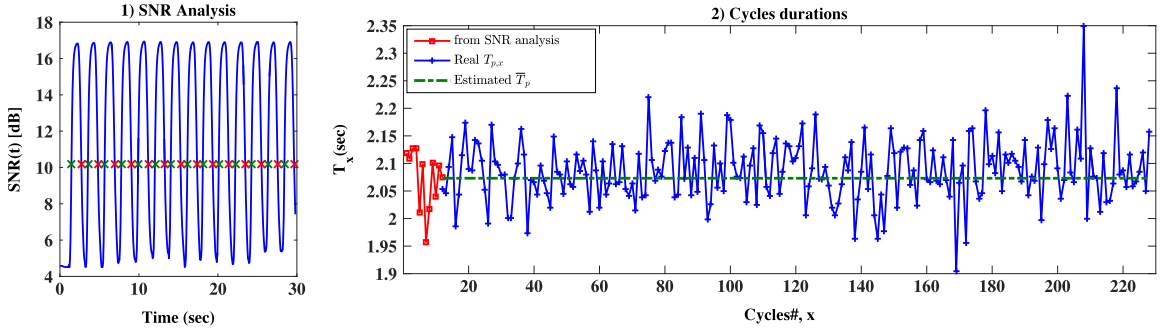

(a) Age: 2 years, $\overline{T}_p = 2.07$ s, MAPE = 1.7%.

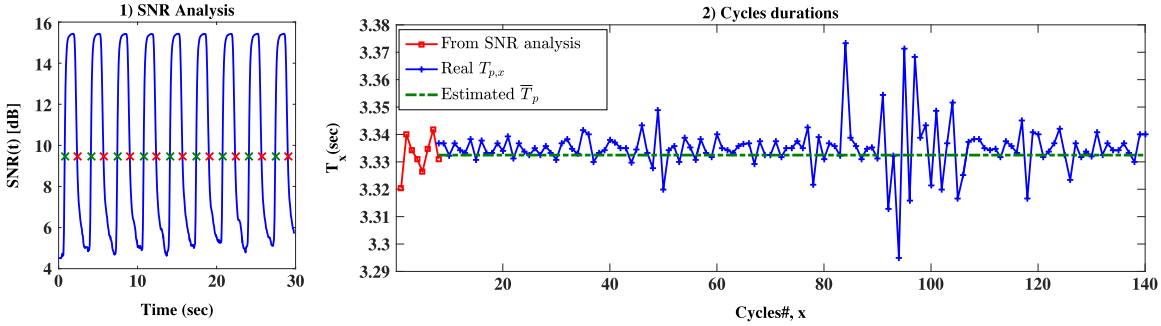

(b) Age: 12 years, $\overline{T}_p = 3.334$ s, MAPE = 0.2%.

Fig. 9. (1) Respiration period approximation based on rises/falls times of the signal and (2) estimated cycle period (green dot curve) from SNR analysis (red curve) along with the real cycle periods (blue curve) for two persons (a and b). (For interpretation of the references to color in this figure legend, the reader is referred to the web version of this article.)

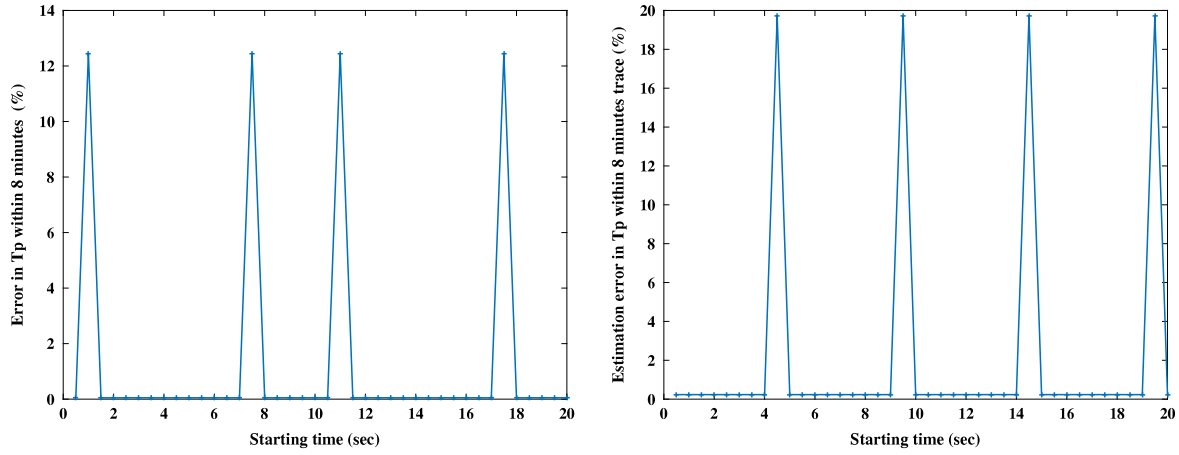

(a) Average MAPE = 1.2%.

(b) Average MAPE = 2.1%.

Fig. 10. The average error when the starting point of the algorithm varies for two subjects.

extract their 8 min capnogram traces. Fig. 9 shows the output of the proposed period detection Algorithm (1) along with the estimated and real cycle periods (2) for two subjects. We see that the algorithm works very well and can detect all the cycles. MAPE for the first subject is 1.7% and for the second subject is only 0.2%. However, the accuracy of the period detection can be affected by the starting points of the algorithm because it may only meet a fraction of a full cycle at the beginning which will not be counted. In order to obtain more insight into this matter, we test the algorithm by shifting the starting point incrementally by 0.2 s up to 20 s and each time measure the accuracy. Fig. 10 shows that in around 4% of the times the error increase significantly but the overall average error is less than 2% for these two cases. Our investigation over 15 subjects shows that the overall error in estimating the respiration periods is less than 1.5%, i.e., we can achieve an accuracy of 98.5%.

6.2. Power reduction by sweet spot exploitation

The goal of this section is to evaluate the required power to target a reliable communication (BER $< 10^{-6}$) over a single-hop communication between nanocollectors and the nanosink when sweet spot is exploited and compare it against the default case when nanosensors are allowed to transmit at any arbitrary time. Taking the typical dimensions of each lung into consideration, the distance between nanosink and nanocollectors could vary from less than 1 mm to around 10 cm. We show the performance of both policies (default and sweet spots) over different distances but our target is a single-hop communication over an average distance equal to 5 cm. We achieve this by using a 60 s respiratory data trace of a 12 year old subject from CapnoBase database [49]. This trace contains 18 respiration cycles and CO_2 data for every 100 ms

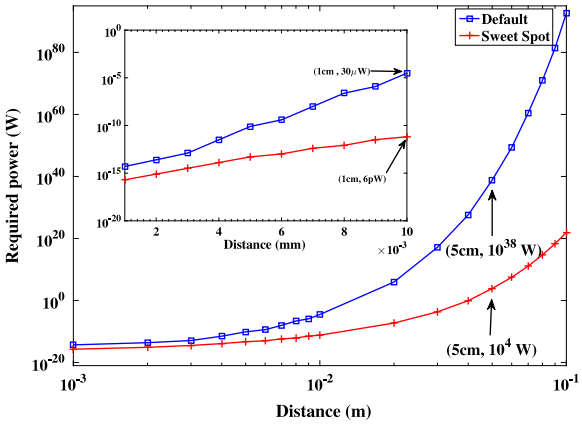

Fig. 11. The required transmission power to secure reliable communication (BER $< 10^{-6}$) over different distances using via both default and sweet spots (20%) modes.

of the trace giving a total of 600 data points. We follow steps explained in Section 4.2 and use Eq. (9) to compute average BER for a given transmission power and communication distance ranging from less than 1 mm to 10 cm. First, we start with a very low power of 1 aW (10^{-18}) and calculate the average BER. While we use all the 600 data points to calculate the average BER for the default mode, for sweet spot exploitation, only a subset of data points that are estimated as sweet spots are used. Then, in a while loop we incrementally increase the power to achieve BER lower than the target BER (10^{-6}).

First, we show the required power for both default and 20% sweet spot over 20 different distances ranging from 1 mm to 10 cm which has been depicted in Fig. 11. As it can be seen from the insert graph, which highlights the results for distances less than or equal to 1 cm, the maximum required power to reliably communicate with the sink for distances less than 1 cm is respectively 30 μW and 6 pW using default and sweet spots. It shows that communication over only sweet spots can drastically reduce the power requirement by more than six orders of magnitudes over distances less than 1 cm. Although the required power for distances less than 1 cm (6 pW) is affordable by the nanocollectors, sweet spots over longer distances needs extremely high power which is due to extremely high path loss in higher distances (Eq. (3)). For example, reliable communication over our target average distance (5 cm) needs a transmission power around 10^8 W which is definitely impossible for the power-restricted nanocollectors. We can either limit the coverage of our proposed lung monitoring system to only distances less than 1 cm far from the nanosinks or alternatively explore new mechanisms that can further improve the power requirement.

In the next section, we introduce another technique which can offer reliable communication in higher distances by selecting the appropriate communication frequency regions which holds the lowest absorption.

6.3. Further power reduction using subband

As we discussed in Section 4, absorption in the terahertz band is sensitive to both frequency and molecular composition of the channel. The *temporal sweet spot* opportunity is based on the observation that molecular composition was variable over time within a respiration cycle. In this section, our goal is to conduct a frequency-dependent absorption analysis for the entire terahertz band to identify possible existence of *frequency sweet spot*, i.e., a frequency subband that provides lower absorption coefficient than the rest of the terahertz band. Existence of such frequency subbands will then provide further opportunities to reduce transmission power by selecting the right subband for communication [10].

We therefore divide the investigated terahertz band (0.1–1.8 THz) to eighty subbands equally spaced each with around 20 GHz bandwidth (the first subband is 0.1–0.12 THz and the last one is 1.78–1.8 THz). Fig. 12 shows one respiration cycle and the corresponding *absorption spectrogram* as a heat map (best viewed in color) where as with high absorption are shown as "hot". We see that the higher frequencies have significantly higher absorption almost all the time. The first subband, 0.1–0.12 THz, experiences the lowest absorption among all other subbands.

Fig. 13 compares power savings using 20% sweet spot exploitation for the entire 0.1–1.8 THz band against the case when only the subband 0.1–0.12 THz is used for communication at a distance equal to 5 cm. First, we see that for the default case (no sweet spot exploitation), use of subband 0.1–0.12 THz reduces transmission power from 10^{38} W to only 0.24 μW which is although a huge power saving (around 35 orders of magnitude) but still very high for nanocollectors. Second, exploitation of sweet spot in the 0.1–0.12 THz subband bring the transmission power requirement for nanocollectors to only 3 pW (3×10^{-12}) which is an affordable power for nanocollectors over a promising distance (5 cm) for single-hop communication, advancing cell-level lung monitoring closer to reality.

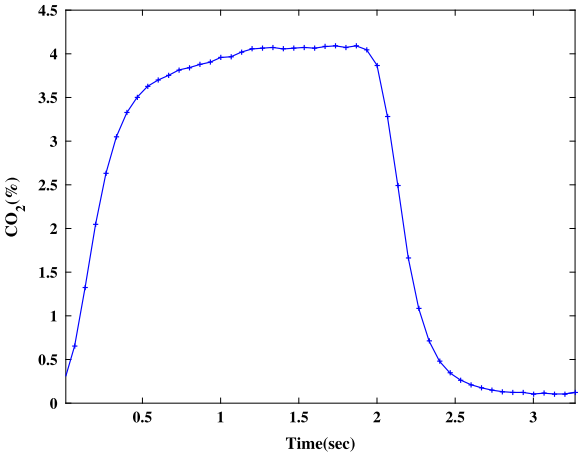

(a) Capnogram.

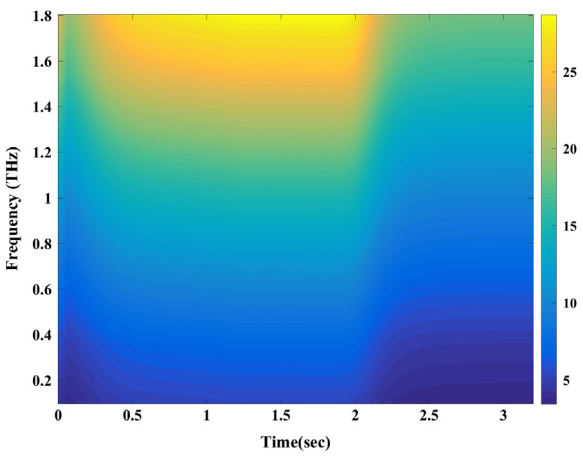

(b) $K(t, f)$ (cm^{-1}).

Fig. 12. (a) Capnogram over one respiration cycle (CO_2 variation) and (b) corresponding absorption spectrogram. (For interpretation of the references to colour in this figure legend, the reader is referred to the web version of this article.)

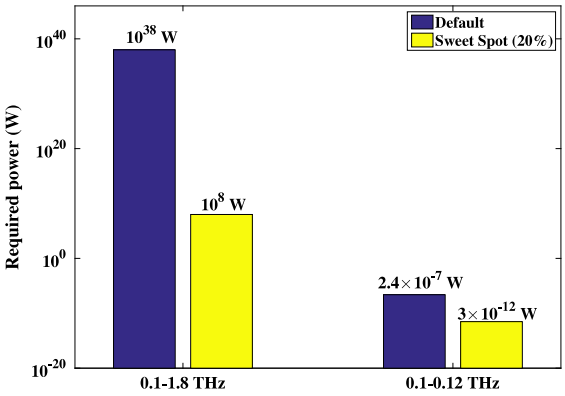

Fig. 13. Power saving due to sweet spot exploitation and selecting appropriate frequency subband for communication at a distance equal to 5 cm.

Our investigation shows that the communication over a narrower subband of 100–102 GHz will further reduce the power requirement of the default mode to around 1 nano watts which is a reasonable power level for the nanosinks to broadcast the periodic beacons across the lung. This narrow subband is also quite sufficient to guarantee the required capacity for the nanosink to transmit 10 small sized beacons per second.

Our discussion in this section has focused on choosing a sub-band which reduces the power requirement for our proposed WNSN. We would like to make a remark on the impact of the sub-band on the form factor of the WNSN node. Past research on the design of graphene-based nano-antenna has shown that the resonance frequency of such antennas is a function of the dimension of the antenna as well as other factors such as chemical potential [4,63–65]. For example, the paper [4] studied the property of a nano-patch antenna using an Armchair Graphene Nanoribbon as the active element. In particular it studied for a patch antenna with width of 50 nm, the length of the antenna is a decreasing function of the resonance frequency if the transverse electric mode is used. This means that if a resonance frequency around 100–102 GHz is needed, the length of the antenna may be around hundreds of micrometers [4, Figure 6b]. However, if the transverse magnetic mode is used, the resonance frequency is a very sensitive function of the length where a change of length of 50 nm can create a change of resonance frequency of hundreds of Terahertz [R1, Figure 6c]. This means that the dimension of the antenna has to be very tightly controlled and it may be difficult to achieve a very narrow band signal. This discussion shows that in order to achieve a resonance frequency of 100–102 GHz, we will need to use the transverse electric mode with one dimension in nanoscale and the other dimension in milli or micro-scale.

6.4. The correlation of transmission window and η

The number of data points inside sweet spot is an increasing function of the percent of the total cycle time the sweet spot occupies, which is controlled by parameter η. Fig. 14(a) shows how the transmission opportunity can be controlled by η parameters.

In our previous results, we assume a transmission window equal to 20% which is obtained by assuming η equal to 1.04. Now, we analyze the transmission power requirement for a BER target of 10^{-6} as a function of sweet spot percentage for communication over 0.1–0.12 THz and distance equal to 5 cm (see Fig. 14(b)). As expected, power requirement decreases as we consider narrower sweet spots. Note that for any transmission opportunity, the target BER (10^{-6}) is met. Therefore, despite using smaller power with narrower sweet spots, capacity is not affected. The exact choice of sweet spot width should depend on the real-time nature of the application. For lung monitoring application, storing a few sensor data in a buffer and transmitting them during sweet spots of each cycle should still provide useful real-time knowledge of the status of the lung.

7. Conclusion

We have presented the concept of a WNSN for monitoring human lung cells and analyzed the transmission power requirements for nanosensors. Our analysis has revealed that terahertz channel quality within human lung is a periodic signal modulated by the respiratory process. We have discovered a temporal sweet spot in the respiration cycle that can be exploited to significantly reduce transmission power of nanosensors. We have proposed a simple online algorithm to estimate the periodic channel and sweet spots exploitation demonstrated that the proposed algorithm can accurately estimate the period and sweet spots of the channel, which allows a significant power reduction. We have also shown that restricting communication to the lower frequencies of the terahertz band enables further power reduction. With these power savings, nanosensors could upload data to a sink in a single hop of 5 cm with only a few pico watts, advancing the concept of cell-level lung monitoring closer to reality.

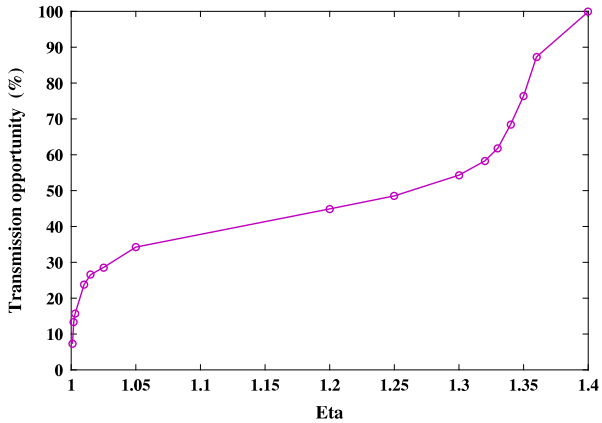

(a) The relationship between η and transmission opportunity.

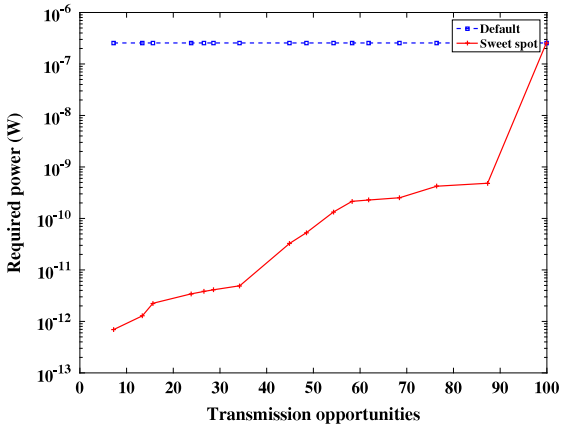

(b) Transmission opportunity vs. required power to target a BER of 10^{-6}.

Fig. 14. The effect of eta on the transmission opportunity and the required power to target BER $< 10^{-6}$.

References

[1] J. Riu, A. Maroto, F. Rius, Nanosensors in environmental analysis, Talanta 69 (2) (2006) 288–301.

[2] F. Dressler, S. Fischer, Connecting in-body nano communication with body area networks: Challenges and opportunities of the Internet of nano things, Nano Commun. Netw. 6 (2) (2015) 29–38.

[3] G. von Maltzahn, J.-H. Park, K.Y. Lin, N. Singh, C. Schwppe, R. Mesters, W.E. Berdel, E. Ruoslahti, M.J. Sailor, S.N. Bhatia, Nanoparticles that communicate in vivo to amplify tumour targeting, Nature Mater. 10 (7) (2011) 545–552.

[4] J. Jornet, I. Akyildiz, Graphene-based plasmonic nano-antenna for terahertz band communication in nanonetworks, IEEE J. Sel. Areas Commun. 31 (12) (2013) 685–694.

[5] A. Afsharinejad, A. Davy, B. Jennings, Frequency selection strategies under varying moisture levels in wireless nano-networks, in: Proceedings of ACM The First ACM International Conference on Nanoscale Computing and Communication, 2014.

[6] A. Afsharinejad, A. Davy, B. Jennings, S. Balasubramaniam, GA-based frequency selection strategies for graphene-based nano-communication networks, in: 2014 IEEE International Conference on Communications (ICC), June 2014, pp. 3642–3647.

[7] I.T. Javed, I.H. Naqvi, Frequency band selection and channel modeling for WNSN applications using simplenano, in: Proceeding of the 2013 IEEE International Conference on Communications (ICC), IEEE, 2013, pp. 5732–5736.

[8] J. Kokkoniemi, J. Lehtomaki, K. Umebayashi, M. Juntti, Frequency and time domain channel models for nanonetworks in terahertz band, IEEE Trans. Antennas and Propagation 63 (2) (2015) 678–691.

[9] I. Llatser, A. Mestres, S. Abadal, E. Alarcon, H. Lee, A. Cabellos-Aparicio, Time- and frequency-domain analysis of molecular absorption in short-range terahertz communications, IEEE Antennas Wirel. Propag. Lett. 14 (2015) 350–353.

[10] E. Zarepour, M. Hassan, C.T. Chou, A. Adesina, Frequency hopping strategies for improving terahertz sensor network performance over composition varying channels, in: The IEEE WoWMoM 2014, Sydney, Australia, June, 2014.

[11] E. Zarepour, M. Hassan, C.T. Chou, A. Adesina, M. Ebrahimi, Reliability analysis of time-varying wireless nanoscale sensor networks, in: The Proceedings of 15th IEEE Conference on Nanotechnology, IEEE-NANO, Rome, Italy, July 2015.

[12] E. Zarepour, M. Hassan, C.T. Chou, A.A. Adesina, Nano-scale sensor networks for chemical catalysis, in: The Proceedings of the 13th IEEE International Conference on Nanotechnology, Beijing, China, 2013.

[13] E. Zarepour, M. Hassan, C.T. Chou, B. Siavash, Performance analysis of carrier-less modulation schemes for wireless nanosensor networks, in: The Proceedings of 15th IEEE Conference on Nanotechnology, IEEE-NANO, Rome, Italy, July 2015.

[14] E. Zarepour, M. Hassan, C.T. Chou, A.A. Adesina, Open-loop power adaptation in nanosensor networks for chemical reactors, IEEE Trans. Mol. Biol. Multi-Scale Commun. 1 (3) (2016) 20–31.

[15] S.J. Lee, C.A. Jung, K. Choi, S. Kim, Design of wireless nanosensor networks for intrabody application, Int. J. Distrib. Sens. Netw. 2015 (2015) 90:90–90:90.

[16] G. Piro, K. Yang, G. Boggia, N. Chopra, L.A. Grieco, A. Alomainy, Terahertz communications in human tissues at the nanoscale for healthcare applications, IEEE Trans. Nanotechnol. 14 (3) (2015) 404–406.

[17] E. Zarepour, M. Hassan, C.T. Chou, M. Ebrahimi Warkiani, Design and analysis of a wireless nanosensor network for monitoring human lung cells, in: Proceedings of the 10th International Conference on Body Area Networks, BodyNets'15, Sydney, Australia, 2015.

[18] I.F. Akyildiz, J.M. Jornet, Electromagnetic wireless nanosensor networks, Nano Commun. Netw. 1 (1) (2010) 3–19.

[19] E. Zarepour, A.A. Adesina, M. Hassan, C.T. Chou, Innovative approach to improving gas-to-liquid fuel catalysis via nanosensor network modulation, Ind. Eng. Chem. Res. 53 (14) (2014) 5728–5736.

[20] P.J. Mazzone, X.-F. Wang, Y. Xu, T. Mekhail, M.C. Beukemann, J. Na, J.W. Kemling, K.S. Suslick, M. Sasidhar, Exhaled breath analysis with a colorimetric sensor array for the identification and characterization of lung cancer, J. Thorac. Oncol. 7 (1) (2012) 137–142.

[21] P. Paredi, S.A. Kharitonov, P.J. Barnes, Analysis of expired air for oxidation products, Am. J. Respir. Crit. Care. Med. 166 (supplement_1) (2002) S31–S37.

[22] A.G. Dent, T.G. Sutedja, P.V. Zimmerman, Exhaled breath analysis for lung cancer, J. Thorac. Dis. 5 (Suppl 5) (2013) S540–S550. jtd-05-S5-S540[PII].

[23] M. Phillips, K. Gleeson, J.M.B. Hughes, J. Greenberg, R.N. Cataneo, L. Baker, W.P. McVay, Volatile organic compounds in breath as markers of lung cancer: a cross-sectional study, Lancet 353 (9168) (1999) 1930–1933.

[24] C. Wang, R. Dong, X. Wang, A. Lian, C. Chi, C. Ke, L. Guo, S. Liu, W. Zhao, G. Xu, E. Li, Exhaled volatile organic compounds as lung cancer biomarkers during one-lung ventilation, Sci. Rep. 4 (2014).

[25] C.W. Na, H.-S. Woo, J.-H. Lee, Design of highly sensitive volatile organic compound sensors by controlling nio loading on zno nanowire networks, RSC Adv. 2 (2012) 414–417.

[26] Y. Paska, T. Stelzner, S. Christiansen, H. Haick, Enhanced sensing of nonpolar volatile organic compounds by silicon nanowire field effect transistors, ACS Nano 5 (7) (2011) 5620–5626. PMID: 21648442.

[27] G. Peng, M. Hakim, Y. Broza, S. Billan, R. Abdah-Bortnyak, A. Kuten, U. Tisch, H. Haick, Detection of lung, breast, colorectal, and prostate cancers from exhaled breath using a single array of nanosensors. Br. J. Cancer, 103 (5):542–551, 2010-08-10 00:00:00.0.

[28] K.-T. Tang, C.-H. Li, S.-W. Chiu, An electronic-nose sensor node based on a polymer-coated surface acoustic wave array for wireless sensor network applications, Sensors (Basel) 11 (5) (2011) 4609–4621. sensors-11-04609[PII].

[29] S. Lenaghan, Y. Wang, N. Xi, T. Fukuda, T. Tarn, W. Hamel, M. Zhang, Grand challenges in bioengineered nanorobotics for cancer therapy, IEEE Trans. Biomed. Eng. 60 (3) (2013) 667–673.

[30] G.-T. Hwang, M. Byun, C.K. Jeong, K.J. Lee, Flexible piezoelectric thin-film energy harvesters and nanosensors for biomedical applications, Adv. Healthc. Mater. 4 (5) (2015) 646–658.

[31] C.R. Yonzon, D.a. Stuart, X. Zhang, A.D. McFarland, Towards advanced chemical and biological nanosensors-An overview, Talanta 67 (3) (2005) 438–448.

[32] E.U. Stutzel, M. Burghard, K. Kern, F. Traversi, F. Nichele, R. Sordan, Data storage: A graphene nanoribbon memory cell, Small 6 (24) (2010) 2821–2830.

[33] M. Fuechsle, J.a. Miwa, S. Mahapatra, H. Ryu, S. Lee, O. Warschkow, L.C.L. Hollenberg, G. Klimeck, M.Y. Simmons, A single-atom transistor, Nature Nanotechnology 7 (4) (2012) 242–246.

[34] Respiration and alveoli of the Lungs, http://hyperphysics.phy-astr.gsu.edu/hbase/ptens2.html and http://hyperphysics.phy-astr.gsu.edu/hbase/biology/respir.html.

[35] U. Yogeswaran, S.-M. Chen, A review on the electrochemical sensors and biosensors composed of nanowires as sensing material, Sensors 8 (1) (2008) 290.

[36] Y. Jie, N. Wang, X. Cao, Y. Xu, T. Li, X. Zhang, Z.L. Wang, Self-powered triboelectric nanosensor with poly(tetrafluoroethylene) nanoparticle arrays for dopamine detection, ACS Nano 9 (8) (2015) 8376–8383. PMID: 26212665.

[37] Z. Kang, Y. Gu, X. Yan, Z. Bai, Y. Liu, S. Liu, X. Zhang, Z. Zhang, X. Zhang, Y. Zhang, Enhanced photoelectrochemical property of zno nanorods array synthesized on reduced graphene oxide for self-powered biosensing application, Biosens. Bioelectron. 64 (2015) 499–504.

[38] A.N. Sekretaryova, V. Beni, M. Eriksson, A.A. Karyakin, A.P.F. Turner, M.Y. Vagin, Cholesterol self-powered biosensor, Anal. Chem. 86 (19) (2014) 9540–9547. PMID: 25164485.

[39] G. Valds-Ramrez, Y.-C. Li, J. Kim, W. Jia, A.J. Bandodkar, R. Nuez-Flores, P.R. Miller, S.-Y. Wu, R. Narayan, J.R. Windmiller, R. Polsky, J. Wang, Microneedle-based self-powered glucose sensor, Electrochem. Commun. 47 (2014) 58–62.

[40] R. Yu, C. Pan, J. Chen, G. Zhu, Z.L. Wang, Enhanced performance of a zno nanowire-based self-powered glucose sensor by piezotronic effect, Adv. Funct. Mater. 23 (47) (2013) 5868–5874.

[41] J.-H. Kim, J. Chun, J.W. Kim, W.J. Choi, J.M. Baik, Self-powered, room temperature electronic nose based on triboelectrification and heterogeneous catalytic reaction, Adv. Funct. Mater. (2015) pages n/a–n/a.

[42] Z. Li, G. Zhu, R. Yang, A.C. Wang, Z.L. Wang, Muscle-driven in vivo nanogenerator, Adv. Mater. 22 (23) (2010) 2534–2537.

[43] G.-T. Hwang, D. Im, S.E. Lee, J. Lee, M. Koo, S.Y. Park, S. Kim, K. Yang, S.J. Kim, K. Lee, K.J. Lee, In vivo silicon-based flexible radio frequency integrated circuits monolithically encapsulated with biocompatible liquid crystal polymers, ACS Nano 7 (5) (2013) 4545–4553. PMID: 23617401.

[44] B.J. Hansen, Y. Liu, R. Yang, Z.L. Wang, Hybrid nanogenerator for concurrently harvesting biomechanical and biochemical energy, ACS Nano 4 (7) (2010) 3647–3652. PMID: 20507155.

[45] W.J.P.D. Marshall, S.K. Bangert, Clinical Chemistry, fifth ed., Mosby, Edinburgh; New York, 2004, Includes index.

[46] J. Jornet, I. Akyildiz, Channel modeling and capacity analysis for electromagnetic wireless nanonetworks in the terahertz band, IEEE Trans. Wireless Commun. 10 (10) (2011) 3211–3221.

[47] W. Lindh, M. Pooler, C. Tamparo, B. Dahl, Delmars Clinical Medical Assisting, Cengage Learning, 2013.

[48] CapnoBase, http://www.capnobase.org/.

[49] W. Karlen, S. Raman, J.M. Ansermino, G.A. Dumont, Multiparameter respiratory rate estimation from the photoplethysmogram, IEEE Trans. Biomed. Eng. 60 (7) (2013) 1946–1953.

[50] E. Gabriel, T. Salerno, Principles of Pulmonary Protection in Heart Surgery, Springer, London, 2010.

[51] D. Hess, N. MacIntyre, W. Galvin, S. Mishoe, Respiratory Care: Principles and Practice, Jones & Bartlett Learning, 2015.

[52] Y.L. Babikov, I.E. Gordon, S.N. Mikhailenko, "HITRAN on the Web", a new tool for HITRAN spectroscopic data manipulation, in: The Proceeding of the ASA-HITRAN Conference, Reims, FRANCE, 2012.

[53] C. Reid, G. Reese, A. Gibson, V. Wallace, Terahertz time-domain spectroscopy of human blood, IEEE J. Biomed. Health Inform. 17 (4) (2013) 774–778.

[54] W.G. Yeo, Terahertz Spectroscopic Characterization and Imaging for Biomedical Applications (Ph.D. thesis), 2015.

[55] I.F. Akyildiz, J.M. Jornet, C. Han, Terahertz band: Next frontier for wireless communications, Phys. Commun. 12 (2014) 16–32.

[56] P. Boronin, D. Moltchanov, Y. Koucheryavy, A molecular noise model for thz channels, in: 2015 IEEE International Conference on Communications, ICC, June 2015, pp. 1286–1291.
[57] J.M. Jornet, I.F. Akyildiz, Femtosecond-long pulse-based modulation for terahertz band communication in nanonetworks, IEEE Trans. Commun. 62 (5) (2014) 1742–1754.
[58] J. Proakis, Digital Communications, fourth ed., McGraw-Hill Education, New York, USA, 2001.
[59] M.S. Hedrick, S.S. Hillman, R.C. Drewes, P.C. Withers, Pulmonary compliance and lung volume varies with ecomorphology in anuran amphibians: implications for ventilatory-assisted lymph flux, J. Exp. Biol. 214 (Pt 19) (2011) 3279–3285.
[60] S. Sundaram, P. Elakkumanan, R. Sridhar, High speed robust current sense amplifier for nanoscale memories: a winner take all approach. in: 19th International Conference on VLSI Design, 2006. Held Jointly with 5th International Conference on Embedded Systems and Design., Jan 2006, p. 6.
[61] Y.C. Yang, F. Pan, Q. Liu, M. Liu, F. Zeng, Fully room-temperature-fabricated nonvolatile resistive memory for ultrafast and high-density memory application, Nano Lett. 9 (4) (2009) 1636–1643. PMID: 19271714.
[62] Y. Ouyang, Y. Yoon, J.K. Fodor, J. Guo, Comparison of performance limits for carbon nanoribbon and carbon nanotube transistors, Appl. Phys. Lett. 89 (20) (2006).
[63] I. Llatser, C. Kremers, A. Cabellos-aparicio, E. Alarcn, D.N. Chigrin, Comparison of the resonant frequency in graphene and metallic nano-antennas, 2012.
[64] M. Tamagnone, J.S. Gmez-Daz, J.R. Mosig, J. Perruisseau-Carrier, Analysis and design of terahertz antennas based on plasmonic resonant graphene sheets, J. Appl. Phys. 112 (11) (2012).
[65] S. Abadal, I. Llatser, A. Mestres, H. Lee, E. Alarcn, A. Cabellos-Aparicio, Time-domain analysis of graphene-based miniaturized antennas for ultra-short-range impulse radio communications, IEEE Trans. Commun. 63 (4) (2015) 1470–1482.

Eisa Zarepour is a Post-doctoral Research Associate in Sharif University of Technology, Tehran, Iran and Visiting Fellow in the School of Computer Science and Engineering, University of New South Wales (UNSW), Sydney, Australia. He received his Ph.D. on designing efficient communication protocols for wireless nanoscale sensor networks from the School of Computer Science and Engineering, UNSW, Sydney, Australia. He also received the Bachelor's degrees in computer engineering from the University of Razi, Kermanshah, Iran and the Master degree in software engineering from Sharif University of Technology, Tehran, Iran in 2003 and 2006, respectively. His research interest is mainly in the area of networking, specializing in designing efficient communication protocols for wireless nanoscale sensor networks, biomedical and bioinformatics.

Mahbub Hassan is a Full Professor in the School of Computer Science and Engineering, the University of New South Wales, Sydney, Australia. He is a Distinguished Lecturer of IEEE (COMSOC) for 2013 to 2016. He was a Keynote Speaker for 2011 ACIS International Conference on Software Engineering, Artificial Intelligence, Networking and Parallel/Distributed Computing and 2009 IEEE International Workshop on Vehicular Networking. He worked as Visiting Professor at Osaka University, Japan, University of Nantes, France, and National ICT Australia. He was a tutorial speaker at IEEE ICC 2012 and IEEE VTC 2011. He is currently an Editor of IEEE Communications Surveys and Tutorial and has previously served as Guest Editor for IEEE Network and Associate Technical Editor for IEEE Communications Magazine. He has co-authored three books on Communication Networks, one US patent, and over 100 refereed articles. Professor Hassan has earned a Ph.D. from Monash University, Australia, and an M.Sc. from University of Victoria, Canada, both in Computer Science and Engineering. More information about Professor Hassan is available from http://www.cse.unsw.edu.au/~mahbub.

Chun Tung Chou is an Associate Professor at the School of Computer Science and Engineering, University of New South Wales, Sydney, Australia. He received his B.A. in Engineering Science from University of Oxford and his Ph.D. in Control Engineering from the University of Cambridge. He has published over 150 articles on various topics, including, systems and control, wireless networks, and communications. His current research interests are molecular communication, nano-scale communication, compressive sensing and embedded networks.

Majid Ebrahimi Warkiani is a lecture at the School of Mechanical and Manufacturing Engineering and an emerging leader in the field of Microfluidic and Nanotechnology. He received his Ph.D. in Mechanical Engineering from Nanyang Technological University (NTU), and undertook postdoctoral training at Massachusetts Institute of Technology (SMART centre). Dr. Warkiani's current research activities focus on three key areas of (i) Microfluidics involving the design and development of novel platforms for rare cells sorting and the development of novel 3D devices for investigation of angiogenesis and tumor formation, (ii) Bio-MEMS involving the fabrication and characterization of novel isopore membranes and the design and development of novel micro PCR chips, and (iii) Rapid prototyping and Tissue engineering involving novel filtration platforms and desktop tumor modeling for drug efficacy screening. Dr Warkiani is also affiliated with the Australian Centre for NanoMedicine (ACN) and Ingham Institute for Biomedical Research at UNSW.